Hyaluronan is abundant in COVID-19 respiratory secretions

Gernot Kaber[1*], Michael J. Kratochvil[1,2*], Elizabeth B. Burgener[1], Egan L. Peltan[1], Graham Barlow[1], Samuel Yang[3], Mark R. Nicolls[4], Vinicio A. de Jesus Perez[4], Joelle Rosser[1], Andrew J. Wardle[1], Anissa Kalinowski[1], Michael G. Ozawa[5], Donald P. Regula[5], Nadine Nagy[1], Sarah C. Heilshorn[2], Carlos E. Milla[6], Angela J. Rogers[4#], and Paul L. Bollyky[1#].

[1] Division of Infectious Diseases and Geographic Medicine, Dept. of Medicine, Stanford University School of Medicine, Beckman Center, 279 Campus Drive, Stanford, CA 94305

[2] Department of Materials Science and Engineering, Stanford University, 476 Lomita Mall, Stanford, CA 94305

[3] Department of Emergency Medicine, Stanford University School of Medicine

[4] Department of Pulmonology and Critical Care Medicine, Stanford University School of Medicine, Lane 235, 300 Pasteur Drive, Stanford, CA 94305

[5] Department of Pathology, Stanford University School of Medicine, Lane 235, 300 Pasteur Drive, Stanford, CA 94305

[6] Center for Excellence in Pulmonary Biology, Department of Pediatrics, Stanford University, 770 Welch Road, Stanford, CA 94305

* Co-first authors

Correspondence to:
Angela J. Rogers, MD, Department of Pulmonology and Critical Care Medicine, Stanford University School of Medicine, Lane 235, 300 Pasteur Drive, Stanford, CA 94305. ajrogers@stanford.edu

Paul Bollyky, MD, PhD: Department of Medicine, Division of Infectious Diseases, Stanford University, 279 Campus Drive, Beckman Center, Stanford CA 94305, USA. pbollyky@stanford.edu

Abbreviations

4-MU	4-methylumbelliferone
ARDS	acute respiratory distress syndrome
CF	cystic fibrosis
HA	hyaluronan
HLF	human lung fibroblasts

Abstract

COVID-19 respiratory infections are associated with copious, adherent respiratory secretions that prolong chronic ventilation and contribute to the morbidity and mortality caused by the disease. We hypothesized that hyaluronan, an extracellular matrix glycosaminoglycan produced at sites of active inflammation that promotes edema in other settings, might be a component of these secretions. To interrogate this, we examined the respiratory secretions collected from eight intubated patients with COVID-19, six control patients with cystic fibrosis (CF), a different respiratory disease also associated with thick adherent secretions, and eight healthy controls. In this sample set we found that hyaluronan content is increased approximately 20-fold in both CF and COVID-19 patients compared to healthy controls. The hyaluronan in COVID-19 samples was comprised of low-molecular weight fragments, the hyaluronan form most strongly linked with pro-inflammatory functions. Hyaluronan is similarly abundant in histologic sections from cadaveric lung tissue from COVID-19 patients. These findings implicate hyaluronan in the thick respiratory secretions characteristic of COVID-19 infection. Therapeutic strategies targeting hyaluronan should be investigated further for potential use in patients with COVID-19.

Keywords: hyaluronan, COVID-19, acute respiratory distress syndrome, sputum

Introduction

The novel coronavirus SARS-CoV-2, a zoonotic pathogen with substantial identity to the known human pathogen SARS-CoV, recently emerged as the cause of a global pandemic. COVID-19 is transmitted primarily through respiratory droplets and appears to drive mortality through acute respiratory distress syndrome (ARDS), a rapid onset respiratory failure characterized by widespread inflammation in the lungs[1,2]. In COVID-19, ARDS manifests as severe hypoxemia that accounts for nearly 85% of COVID-19 related deaths[3]. These patients produce thick, highly viscous respiratory secretions that are difficult to clear and may complicate oxygenation[4]. Analysis focused on the composition of these secretions is important for understanding the pathophysiology of COVID-19 and directing efforts for targeted treatments with strong rationale for efficacy.

It has been previously reported that hyaluronan (HA), a component of the extracellular matrix, is associated with diverse forms of respiratory inflammation[5-9] including ARDS[10,11]. HA is a linear and highly charged polysaccharide known to complex a large number of water molecules[12-14]. Along with driving edema[15], HA plays an important role in inflammation and local immune responses in the lung[16-18]. Stimulation of lung fibroblasts with the cytokines Interleukin-1β, tumor necrosis factor-α, or the viral RNA mimetic poly[I:C] induces the expression of HA synthases and promotes the deposition of HA[19-23]. Following tissue injury, oxidative stress, mechanical force, and enzymatic degradation through hyaluronidases, degrade high-molecular weight (~10^7 Da) HA into smaller low-molecular weight (~10^5 Da) HA[24,25]. These HA fragments are known to function as endogenous danger-associated molecular pattern molecules (DAMPs) that trigger inflammatory responses, through TLR2 and TLR4 signaling, thus promoting inflammation[26-29]. Together this evidence suggests that accumulated HA fragments can promote both local inflammation and further HA synthesis within the lungs.

Given the links of HA to airway inflammation and pulmonary edema, we hypothesized that sputum HA may likewise contribute to the pathophysiology of COVID-19 infection. To test this, we have examined respiratory secretions and autopsy samples from COVID-19 patients. As positive controls for these

patients, we have used induced sputum samples from subjects with cystic fibrosis (CF), a condition also associated with thick, tenacious respiratory secretions[30], as well as heathy controls.

Results

Low molecular weight HA is present in high amounts in COVID-19 sputum

We first asked whether HA is present in the sputum collected from COVID-19 subjects and controls. To this end we collected tracheal aspirations from eight COVID-19 patients (CV). As positive controls, we obtained induced sputum from six CF patients. As negative controls we obtained sputum from eight healthy controls (HC) patients. We observed that sputum HA content was significantly increased in the CF and COVID-19 samples compared to HC samples (**Fig. 1A**). These data indicate that sputum HA content is significantly increased in COVID-19 infection. They also suggest that HA levels in COVID-19 patients are comparable to those seen in CF.

We next assessed HA size in a representative subset of the samples. We observed that COVID-19 sputum samples are dominated by low-molecular weight HA (**Fig. 1B-D**). HA from COVID-19 patients appeared smaller than HA in sputum of CF or HC subjects. Together these data indicate that HA is increased in COVID-19 sputum and that it is dominated by low-molecular weight polymer forms.

HA is present in high quantities in COVID-19 lung tissue

We next asked whether HA is found in histologic sections from cadaveric subjects. To this end, we obtained lung tissue sections and stained these with HA binding peptide' to visualize HA. We observed minimal lung HA in tissue from a subject who died of causes unrelated to respiratory function (**Fig. 1A-C**). We then evaluated lung sections from a patient who died from COVID-19-associated ARDS. We observed extensive occlusion of airway spaces with poorly organized polymeric material that stained robustly for HA (**Fig. 2E**). These areas were seen to be associated with diffuse alveolar infiltrates (**Fig. 2F**). This staining was lost in sections pre-treated with hyaluronidase (HA'ase)(**Fig. 2D**). Substantial HA was also seen in lung tissue collected from a patient who died of respiratory complications associated with CF (**Fig. 2G-I**).

These data suggest that HA is abundant in the airway secretions observed in this patient, consistent with our observation in airway secretions (**Fig. 1)**.

Together these data suggest that human airway cells may produce HA in response to SARS-CoV-2.

Discussion

We report here that HA is greatly increased in sputum samples from intubated COVID-19 patients. Consistent with this, HA is abundant in histologic sections from cadaveric lung tissue obtained from an individual with COVID-19-associated ARDS. Moreover, treatment of human cadaveric lung sections with COVID-19 likewise induced HA production. Together these data support the hypothesis that low-molecular weight HA is elevated in the respiratory secretions of patients with COVID-19-associated ARDS and may be a contributing factor in the inflammatory state in the lungs.

These data link heightened HA production to the thick, viscous long secretions associated with COIVD-19. These data are consistent with reports describing increased HA in ARDS due to other etiologies[10,11]. HA is likewise associated with anti-viral responses[31] and Th1 polarized immunity in other settings[32].

These studies have several limitations. Most notable is the small numbers of cases and samples of sputum involved. These findings need to be confirmed in larger, multi-center studies involving individuals with diverse backgrounds and case presentations. The underlying mechanism of the increased HA we found would also benefit from further research of the cell types and signalling pathways that produce HA in the lung. In addition, data in SARS-CoV-2 animal models would enable improved understanding of the contribution of HA to pathogenesis in this disease.

That stated, given the evidence supporting low molecule weight HA's role in respiratory inflammation, including COVID-19-associated respiratory distress and mortality, further investigation of the utility of agents known to reduce HA content, such as hymecromone, is recommended.

In summary, these data reveal a novel role for HA in COVID-19 respiratory secretions that have important implications for the development of much needed therapeutics for patients with COVID-19.

Methods

Human tissue donors and tissue procurement: We collected discarded tracheal aspirates, which were obtained as part of routine clinical care from seven intubated patients at Stanford University who were enrolled in either the Stanford ICU Biobank, Stanford IRB approval #28205, or the Stanford COVID-19 Biobank, Stanford IRB approval # 55650. Written informed consent was obtained from patients or their surrogates. One pediatric patient from Lucille Packard Hospital and Clinics was enrolled via IRB #43805 via surrogate informed consent. All subjects had a positive SARS-CoV-2 nasopharyngeal swab by RT-PCR. The majority of patients were co-enrolled in ongoing COVID-19 treatment trials at Stanford. The Stanford ICU biobank and Stanford COVID-19 biobank screened new admissions via an electronic medical records review of all COVID-19 positive subjects every day with a goal enrollment within less than 48 h of admission to the hospital, though tracheal aspirates could be collected at a later date. To protect the identity of the COVID-19 subjects, ages are reported as ranges. For controls, sputum was collected from eight asymptomatic adult donors after written informed consent (Stanford IRB approval #37232).

All eight CV-19 samples were collected from ventilated patients who were diagnosed with ARDS as defined by the Berlin Criteria. The 8 COVID-19 patients were aged 15 to 81 years. Five were male, three were female. Samples were collected between 2 and 16 days following hospital admission. HC subjects were asymptomatic, four male and four female, and aged 24–50 years. Sputum samples from CF patients were collected during routine care. HC and CF sputum samples and IRB numbers 37232 and 43805.

All samples were frozen at -80°C immediately after collection and heat inactivated at 65°C for 30 minutes to render them noninfectious prior to further analyses. These studies were approved under APB protocol 2379. Samples from patients with COVID-19 and healthy controls were processed side by side to avoid variation from processing. Human lung tissue was obtained from a de-identified, discarded autopsy specimen provided through the Stanford Pathology Department in the form of formalin-fixed, paraffin-embedded histologic specimen.

HLF were derived from explants of the lung, following removal of both the pleura and parenchyma.. The cells were isolated as described previously in accordance with approval from the institution's human

subjects review committee. HLFs were maintained in DMEM high-glucose medium supplemented with 10% FBS (HyClone; Logan, UT), 1 mM sodium pyruvate, 0.1 mM non-essential amino acids, 0.43 mg/ml GlutMAX-1, and penicillin-streptomycin (penicillin G sodium, 100 U/ml, and streptomycin sulfate, 0.10 mg/ml; Invitrogen) at 37 °C in 5% CO_2. Cells were passaged with trypsin-EDTA (0.05% trypsin and 0.53 mM tetrasodium EDTA) and were used for experiments between passages 9 and 17 after initial isolation.

Quantification and sizing of sputum HA levels: Human sputum samples were thawed and subsequent assayed for HA levels using a modified HA Enzyme-Linked Immunosorbent Assay (ELISA) as previously described[33]. Each sample was analyzed in triplicate.

Sputum samples were treated with 250 U benzonase for 30 min at 37°C for DNase digestion. Followed by an incubation with 1 mg/ml proteinase K for 4 hrs at 60°C for further digestion. Insoluble particles were removed before further processing. Samples were precipitated with ethanol, by adding 4 volumes of pre-chilled 200 proof ethanol to each sample and incubated at -20°C overnight. The following day the samples were centrifuged at 14,000 g for 10 minutes at RT. Supernatant was discarded and the pellet was washed by adding 4 volumes of pre-chilled 75% ethanol. Samples were centrifuged at 14,000 g for 10 minutes; supernatant was discarded and the pellet was air dried at RT for 20 minutes. 100 µl 100 mM ammonium acetate was added to each sample, vortexed and incubated at RT for 20 minutes. Proteinase K was heat inactivated by incubating the samples at 100°C for 5 min,

For the digestion of nucleic acids 6 U DNAse and 3 µl RNAse A was added, samples were digested overnight at 37°C, afterwards enzymes were heat killed in boiling water. 400 µl 200 proof ethanol was added and samples overnight at -20°C. In a second ethanol precipitation, samples were centrifuged, supernatant was discarded, and the pellet was washed with cold 75% ethanol and centrifuged as previously described. The pellet was air dried for 20 min and resuspend in 20 µl 100 mM ammonium acetate (pH 7.0). Samples were lyophilized and resuspend in 10 µl of 10 M formamide. A 1.5% TAE agarose gel was cast and run at 100 V. After the run the gel was stained with stains-all and incubated at RT overnight. The gel was imaged on a BioRad GS-800 Calibrated Densitometer. On the gels twice the volume of healthy control samples was loaded compared to CF and CV.

Histologic staining of lung tissues for HA: This staining was performed as described previously[34]. In brief, 5 µm thick sections were cut on a Leica RM 2255 Microtomes (Leica Microsystems Inc.). All staining steps were performed on a Leica Bond Max™ automated immune histochemistry (IHC) stainer (Leica Microsystems Inc.). For HA affinity histochemistry (AFC) the Bond Intense R Detection kit, a streptavidin-horse radish peroxidase (HRP) system, (Leica Microsystems, Inc.) was used with 4 µg/mL biotinylated-hyaluronan binding protein in 0.1 % BSA-PBS as the primary. The Bond Polymer Detection Kit was used for all other immunohistochemistry. This detection kit contains a goat anti-rabbit conjugated to polymeric HRP and a rabbit anti-mouse post primary reagent for use with mouse primaries. All images were visualized using a Leica DMIRB inverted fluorescence microscope equipped with a Pursuit 4-megapixel cooled color/monochrome charge-coupled device camera (Diagnostic Instruments, Sterling Heights, MI). Images were acquired using the Spot Pursuit camera and Spot Advance Software (SPOT Imaging Solutions; Diagnostic Instruments). Image analysis was performed using Image J (NIH), as described previously[34].

Statistical analysis

Data are expressed as means +/- SEM of n independent measurements. Significance of the difference between the means of two or three groups of data was evaluated using the Mann-Whitney U test or one-way Anova, respectively. The statistical significance of differences in sputum hyaluronan levels was calculated by the Kruskal-Wallis test. Correlation analysis was performed using the non-parametric Spearman correlation test. A p value less than <0.05 was considered statistically significant.

Acknowledgements

Our thanks go to A. Wardle for his reading of the manuscript and his helpful comments. We would also like to thank G. Nolan for providing access to the Keyence microscope and analysis software. We are grateful to all participants in this study.

Funding: This research program is supported by a grant from the Stanford Innovative Medicines Accelerator program. The Stanford ICU Biobank and A.J.R. are funded by NIH/ NHLBI K23 HL125663. The following reagent was deposited by the Centers for Disease Control and Prevention and obtained through BEI Resources, NIAID, NIH: SARS-Related Coronavirus 2, Isolate USA-WA1/2020, NR-52281.

Author contributions: G.K. and P.L.B., conceived the study. C.M., E.B.B, M.G.O., D.P.R., V.A.dJ.P., and A.J.R. identified, enrolled, and consented eligible patients and patient samples. G.K., M.J.K., and P.L.B. processed patient samples. G.K., M.J.K., A.H., G.B., S.E., T.N.W., performed experiments and analyses. G.K., M.J.K., N.N., S.C.H., M.R.N, C.E.M, A.J.R. and P.L.B., interpreted data and wrote the manuscript with input from all authors.

References

1. Thompson, B. T., Chambers, R. C. & Liu, K. D. Acute Respiratory Distress Syndrome. *N. Engl. J. Med.* **377,** 1904–1905 (2017).
2. Matthay, M. A. & Zemans, R. L. The acute respiratory distress syndrome: pathogenesis and treatment. *Annu Rev Pathol* **6,** 147–163 (2011).
3. Ruan, Q., Yang, K., Wang, W., Jiang, L. & Song, J. Clinical predictors of mortality due to COVID-19 based on an analysis of data of 150 patients from Wuhan, China. *Intensive Care Med* **46,** 846–848 (2020).
4. Li, T., Lu, H. & Zhang, W. Clinical observation and management of COVID-19 patients. *Emerg Microbes Infect* **9,** 687–690 (2020).
5. Lauer, M. E., Dweik, R. A., Garantziotis, S. & Aronica, M. A. The Rise and Fall of Hyaluronan in Respiratory Diseases. *Int J Cell Biol* **2015,** 712507–15 (2015).
6. Bai, K.-J. *et al.* The role of hyaluronan synthase 3 in ventilator-induced lung injury. *Am. J. Respir. Crit. Care Med.* **172,** 92–98 (2005).
7. Lazrak, A. *et al.* Hyaluronan mediates airway hyperresponsiveness in oxidative lung injury. *Am. J. Physiol. Lung Cell Mol. Physiol.* **308,** L891–903 (2015).
8. Collum, S. D. *et al.* Adenosine and hyaluronan promote lung fibrosis and pulmonary hypertension in combined pulmonary fibrosis and emphysema. *Dis Model Mech* **12,** dmm038711 (2019).
9. Tesar, B. M. *et al.* The role of hyaluronan degradation products as innate alloimmune agonists. *Am. J. Transplant.* **6,** 2622–2635 (2006).
10. Esposito, A. J., Bhatraju, P. K., Stapleton, R. D., Wurfel, M. M. & Mikacenic, C. Hyaluronic acid is associated with organ dysfunction in acute respiratory distress syndrome. *Crit Care* **21,** 304–8 (2017).
11. Hällgren, R., Samuelsson, T., Laurent, T. C. & Modig, J. Accumulation of hyaluronan (hyaluronic acid) in the lung in adult respiratory distress syndrome. *Am. Rev. Respir. Dis.* **139,** 682–687 (1989).
12. Gibbs, D. A., Merrill, E. W., Smith, K. A. & Balazs, E. A. Rheology of hyaluronic acid. *Biopolymers* **6,** 777–791 (1968).
13. Cowman, M. K., Schmidt, T. A., Raghavan, P. & Stecco, A. Viscoelastic Properties of Hyaluronan in Physiological Conditions. *F1000Res* **4,** 622 (2015).
14. Balazs, E. A. Viscoelastic properties of hyaluronic acid and biological lubrication. *Univ Mich Med Cent J* 255–259 (1968).
15. Nettelbladt, O., Tengblad, A. & Hällgren, R. Lung accumulation of hyaluronan parallels pulmonary edema in experimental alveolitis. *Am. J. Physiol.* **257,** L379–84 (1989).
16. Comper, W. D. & Laurent, T. C. Physiological function of connective tissue polysaccharides. *Physiol. Rev.* **58,** 255–315 (1978).
17. Johnson, P., Arif, A. A., Lee-Sayer, S. S. M. & Dong, Y. Hyaluronan and Its Interactions With Immune Cells in the Healthy and Inflamed Lung. *Front Immunol* **9,** 2787 (2018).
18. Noble, P. W. & Jiang, D. Matrix regulation of lung injury, inflammation, and repair: the role of innate immunity. *Proc Am Thorac Soc* **3,** 401–404 (2006).
19. Wilkinson, T. S., Potter-Perigo, S., Tsoi, C., Altman, L. C. & Wight, T. N. Pro- and anti-inflammatory factors cooperate to control hyaluronan synthesis in lung fibroblasts. *Am. J. Respir. Cell Mol. Biol.* **31,** 92–99 (2004).
20. Mohamadzadeh, M., DeGrendele, H., Arizpe, H., Estess, P. & Siegelman, M. Proinflammatory stimuli regulate endothelial hyaluronan expression and CD44/HA-dependent primary adhesion. *J. Clin. Invest.* **101,** 97–108 (1998).
21. Potter-Perigo, S. *et al.* Polyinosine-polycytidylic acid stimulates versican accumulation in the extracellular matrix promoting monocyte adhesion. *Am. J. Respir. Cell Mol. Biol.* **43,** 109–120 (2010).
22. Evanko, S. P., Potter-Perigo, S., Bollyky, P. L., Nepom, G. T. & Wight, T. N. Hyaluronan and versican in the control of human T-lymphocyte adhesion and migration. *Matrix Biol.* **31,** 90–100 (2012).

23. Lauer, M. E. *et al.* Airway smooth muscle cells synthesize hyaluronan cable structures independent of inter-alpha-inhibitor heavy chain attachment. *J. Biol. Chem.* **284,** 5313–5323 (2009).
24. Teder, P. *et al.* Resolution of lung inflammation by CD44. *Science* **296,** 155–158 (2002).
25. Stern, R. & Jedrzejas, M. J. Hyaluronidases: their genomics, structures, and mechanisms of action. *Chem. Rev.* **106,** 818–839 (2006).
26. McKee, C. M. *et al.* Hyaluronan (HA) fragments induce chemokine gene expression in alveolar macrophages. The role of HA size and CD44. *J. Clin. Invest.* **98,** 2403–2413 (1996).
27. Noble, P. W., McKee, C. M., Cowman, M. & Shin, H. S. Hyaluronan fragments activate an NF-kappa B/I-kappa B alpha autoregulatory loop in murine macrophages. *J. Exp. Med.* **183,** 2373–2378 (1996).
28. Taylor, K. R. *et al.* Hyaluronan fragments stimulate endothelial recognition of injury through TLR4. *J. Biol. Chem.* **279,** 17079–17084 (2004).
29. Scheibner, K. A. *et al.* Hyaluronan fragments act as an endogenous danger signal by engaging TLR2. *J. Immunol.* **177,** 1272–1281 (2006).
30. Ratjen, F. *et al.* Cystic fibrosis. *Nat Rev Dis Primers* **1,** 15010–19 (2015).
31. Reeves, S. R. *et al.* Respiratory Syncytial Virus Infection of Human Lung Fibroblasts Induces a Hyaluronan-Enriched Extracellular Matrix That Binds Mast Cells and Enhances Expression of Mast Cell Proteases. *Front Immunol* **10,** 3159 (2019).
32. Bollyky, P. L. *et al.* Th1 cytokines promote T-cell binding to antigen-presenting cells via enhanced hyaluronan production and accumulation at the immune synapse. *Cell. Mol. Immunol.* **7,** 211–220 (2010).
33. Nagy, N. *et al.* Hyaluronan levels are increased systemically in human type 2 but not type 1 diabetes independently of glycemic control. *Matrix Biol.* (2018). doi:10.1016/j.matbio.2018.09.003
34. Nagy, N. *et al.* Inhibition of hyaluronan synthesis restores immune tolerance during autoimmune insulitis. *J. Clin. Invest.* **125,** 10.1172/JCI79271–0 (2015).

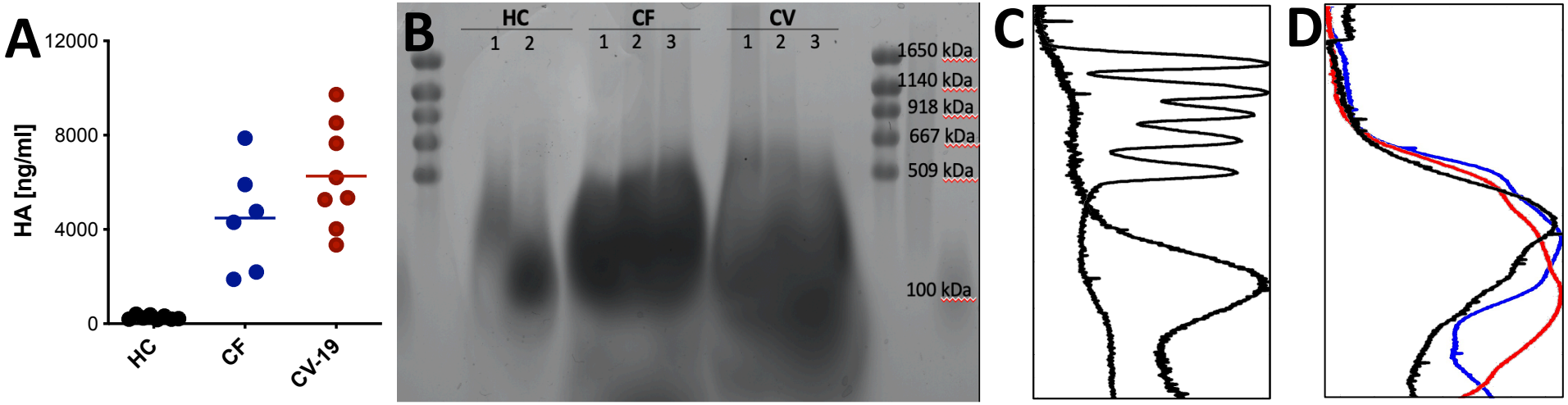

Figure 1. HA is abundant in CV-19 sputum. A. HA content measured in tracheal aspirations collected from CV-19 patients (n = 8), in induced sputum samples from Cystic Fibrosis (CF) patients (n = 6), and in induced sputum samples from HC patients (n = 8). CF cases are provided as a control given that the thick, tenacious respiratory secretions in that disease are similar to those seen in COVID-19. * $p<0.05$ vs HC. Statistics were assessed using One-way ANOVA followed by Tukey's Multiple Comparison Test. **B.** HA sizing of HC, CF, and CV-19 samples with an HA size ladder provided for reference. **C-D.** Densitometry data for the size ladder (**C**) and gel bands (**D**) in (**B**). Data in **B-D** are representative of 3 independent experiments.

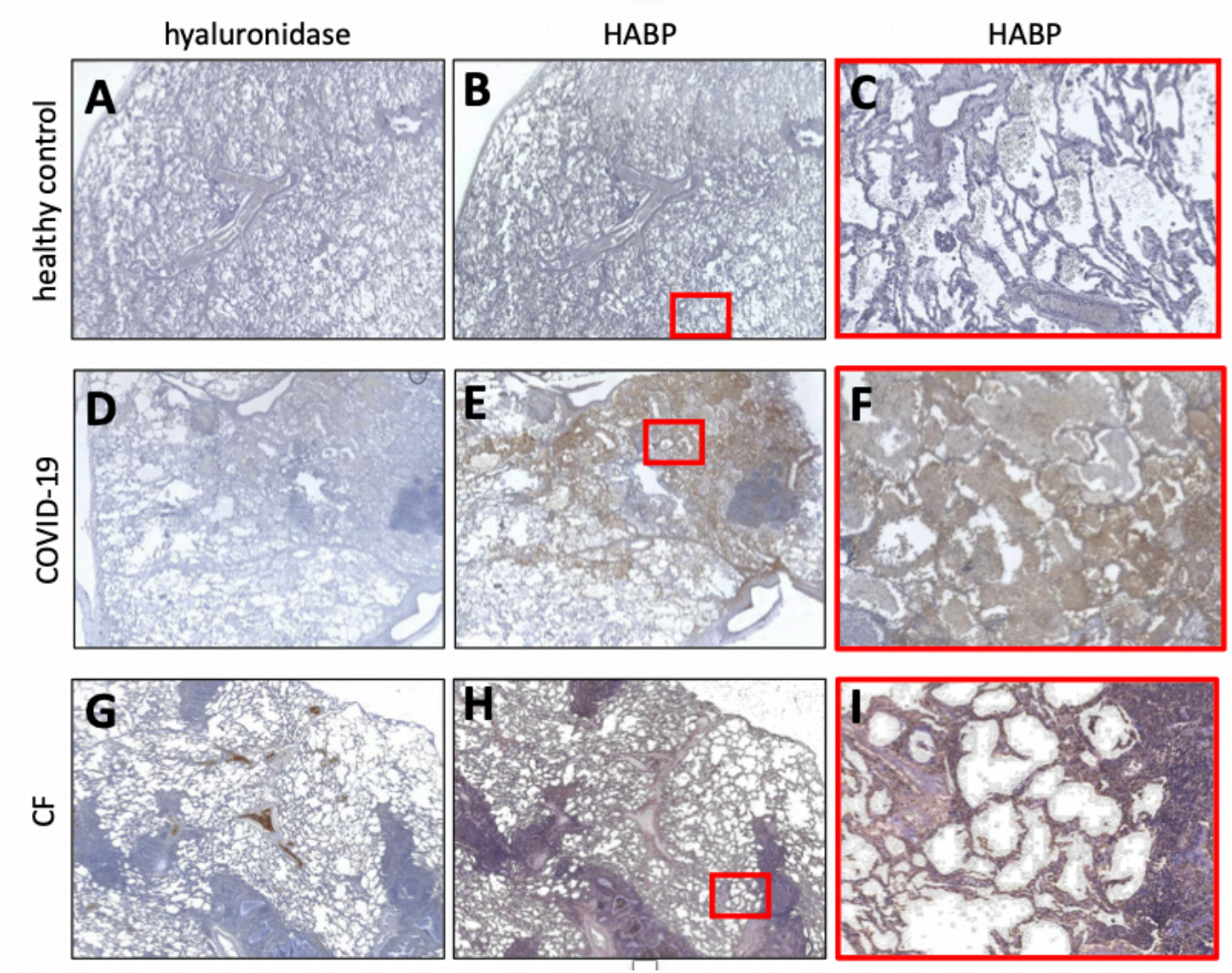

Figure 2. HA is abundant in cadaveric lung tissue from a COVID-19 patient. Lung tissue from representative human subjects who died of issues unrelated to lung disease (**A-C**), of COVID-19 respiratory infection (**D-F**), or of chronic respiratory infections associated with CF (**G-I**) were fixed with formalin and stained with biotinylated HABP. **A,D,G.** Pre-treatment with HA'ase followed by staining with HABP. **B,E,H**. An adjacent section stained for HA with biotinylated HABP. **C,F,I.** High resolution images of the red square in panels **B,E,** and **H,** respectively. .